Structural and electronic properties of the liquid polyvalent elements. III. The trivalent elements

J. Hafner and W. Jank
Institut für Theoretische Physik, Technische Universität Wien, Wiedner Hauptstrasse 8-10, A-1040 Wien, Austria
(Received 03 July 1990)

We present *ab initio* calculations of the atomic structure, the electronic density of states, and the photoemission intensities of the trivalent metals Al, Ga, In, and Tl. The investigations are based on pseudopotential-derived interatomic forces, molecular-dynamics simulations for the atomic structure, and self-consistent linear-muffin-tin-orbital supercell calculations for the electronic structure and photoelectron spectra. This study extends similar work on the liquid di- and tetravalent elements [W. Jank and J. Hafner, Phys. Rev. B **41**, 1497 (1990); **42**, 6926 (1990)]. We show that the trend from a close-packed structure in liquid Al to a somewhat more loosely packed atomic arrangement in liquid Ga, but then a return to more close-packed structure in the heavy elements arises from a modulation of the random packing of atoms by the Friedel oscillations in the potential and the damping of these oscillations by relativistic effects. Relativistic effects are also responsible for the formation of a pseudogap separating the *s*- and *p*-orbital-dominated parts of the valence band.

I. INTRODUCTION

In two recent papers[1,2] (hereafter referred to as I and II) we started a theoretical investigation of the characteristic trends in the structural and electronic properties of the liquid polyvalent elements across the Periodic Table. In I we studied the transition from the open, low-coordinated structures of liquid Si and Ge to the dense, close-packed structures of liquid Sn and Pb, and its relation to the transition from a free-electron-like density of states with strong *s*-*p* hybridization in Si to well-separated *s* and *p* bands in liquid Pb. Paper II was devoted to the investigation of the increasing distortion of the hard-sphere-like structures accompanying the onset of the formation of a pseudogap at the Fermi level in the liquid II-B metals from Mg to Hg, and of the tendency to a transition-metal behavior in the molten alkaline-earth metals. We have demonstrated that in the liquid as well as in the crystalline elements the complex structures of Si and Ge on the one hand and of Hg on the other hand arise from the modulation of the packing (random or crystalline) of atoms by the Friedel oscillations in the interatomic forces. The amplitude of these oscillations is set by the on-Fermi-surface matrix element of the effective ion-electron interaction. The strength of this matrix element is strongly influenced by relativistic effects: in the heavy elements, *s* electrons are more strongly bonded than *p* electrons. This explains the appearance of the *s*-*p* pseudogap in the electronic structure, the damping of the Friedel oscillations, and the return to close-packed atomic structures.

In the present paper we extend our investigations to the trivalent elements. Here the trend in the crystalline and liquid structures is somewhat more complex: first we observe a transition from a close-packed structure in Al (coordination number $N_c=12$ and 11.5 in the crystal and in the melt) to an open, low-coordinated structure in Ga ($N_c=7$ in orthorhombic α-Ga and $N_c=9$–10 in liquid Ga), but then a return to more regular, close-packed structures in In and Tl.[3] Contrary to this nonmonotonic variation in the atomic structures, the electronic densities of states show a gradual transition from a free-electron parabola in liquid Al to a density of states (DOS) with a gap between *s* and *p* bands in liquid and crystalline Tl.[4,5] Our study is based on techniques discussed in detail in the two previous papers: pseudopotential-derived interatomic forces, molecular-dynamics simulation for the atomic structure, and self-consistent linear-muffin-tin-orbital (LMTO) supercell calculations for the electronic densities of states and the photoemission intensity. For the discussion of the technical aspects we refer entirely to I and II. Our results are discussed below.

II. INTERATOMIC FORCES AND ATOMIC STRUCTURE

Aluminum crystallizes in the face-centered cubic structure. Gallium is known to show at least nine solid phases,[6] but the only phase stable at room temperature is the orthorhombic α phase with eight atoms per unit cell. Each atom is coordinated by seven neighbors. Indium crystallizes in a face-centered-tetragonal structure with an axial ratio of $c/a=1.07$. Thallium crystallizes in a hexagonal-close-packed structure at low temperatures and pressures, but transforms to a face-centered-cubic form under elevated pressure and to a body-centered-cubic form at higher temperatures. The trend in the liquid structures follows those in the crystalline metals:

Al is the prototype of a monatomic metallic melt whose structure is rather well described by a dense random packing of hard spheres. Liquid Ga has been extensively studied using neutron and x-ray diffraction.[7-11] The experiments point to a somewhat loose packing with about nine to ten nearest neighbors, reflected in a slight asymmetry of the first peak in the pair-correlation function $g(R)$ and a shoulder in the static structure factor $S(q)$. A change in the local order at melting is also indicated by the anomalous density increase of 3.2%, whereas most metals show a density decrease by 2–6%. Liquid In and Tl are again more densely packed (N_c=11.6 for both metals[2]), only a slight asymmetry in the first peak of $g(R)$ indicates a somewhat irregular atomic arrangement.

The trends in the crystalline structures were interpreted by Hafner and Heine[12,13] in terms of the variation of the effective interatomic interaction with electron density and pseudopotential. This analysis was extended to liquid metals by Hafner and Kahl.[13,14] Their argument is essentially the following: for small electron densities and large core radii [measured in units of the electron density parameter $R_s = (3V_a/4\pi Z)^3$, V_a is the atomic volume and Z the valence], the pair potential has a minimum at the nearest-neighbor distance D_{cp} for close packing, resulting in stable close-packed structures (periodic or random) — here for Al. As the electron density increases and/or the core radius decreases, the minimum is shifted relative to D_{cp} and flattened. This yields distorted structures at first (here for Ga), but then a return to close-packed structures as the last trace of an oscillation in the pair potential at D_{cp} has disappeared (here for Tl). On the lowest level of approximation, using an empty-core pseudopotential, the essential trend may be parametrized in terms of (R_c/R_s), where R_c is the pseudopotential core radius. Within a given group of the Periodic Table (Z=const), the important point is the decrease of (R_c/R_s) at an essentially constant R_s and we refer to the paper by Hafner and Heine[13] for a discussion on how this trend relates to physical effects such as the existence of a d^{10} core and the nonlocality of the pseudopotential of the heavy elements arising from relativistic effects. Our present study shows that the arguments presented by Hafner and Heine are qualitatively correct but quantitatively we find that a precise evaluation of the small distortions of the structure functions of Ga, In, and Tl from a hard-sphere form requires very accurate pair potentials.

The calculation of the effective pair interaction requires the specification of the pseudopotential and of the local-field corrections to the dielectric function of the electron gas. For the local-field corrections we used the Vashishta-Singwi[15] and the Ichimaru-Utsumi[16] forms, both of which satisfy the compressibility sum rule for the electron gas. For the pseudopotential we used both the local Ashcroft[17] empty-core potential and the first-principles optimized pseudopotentials originally developed by Harrison[18] and used in slightly different variants by Hafner,[13,19] Moriarty,[20-22] and others. In this approach exchange and correlation between the core electrons and the core-valence exchange and correlation interactions are described in a local-density-functional framework. Here a certain problem arises from the nonlinearity of the exchange-correlation functional. Subtracting the exchange-correlation potential of the valence electrons from the total exchange-correlation potential leads to (we use atomic units)

$$V_{xc}(r) = -6\alpha\left(\frac{3}{8\pi}\right)\{\,[\rho_{core}(r)+\rho_{val}(r)]^{1/3} - \rho_{val}(r)^{1/3}\} \quad (1)$$

for the core-valence interaction. This procedure represents a linearization of the exchange-correlation potential as a function of the charge density. It is exact by definition for an atomic configuration. If, consistent with the electron-gas screening, ρ_{val} is approximated by a homogeneous density $\rho^0_{val} = Z/V_a$, a systematic error is introduced. This error is small unless ρ_{core} and ρ^0_{val} are of the same order of magnitude, i.e., for the light polyvalent elements. In this case V_{xc} with ρ^0_{val} leads to a systematic underestimate. In our earlier extensive investigations[23,24] of the cohesive and dynamic properties of the crystalline elements we have shown that this can be corrected by choosing a larger coefficient α in V_{xc}. For the electron gas as well as the free atom the Kohn-Sham value $\alpha = \frac{2}{3}$ leads to an accurate exchange potential. We use this value for the calculation of all core wave functions, and for V_{xc} of the heavy elements (In,Tl). For Al we find that a value of $\alpha = 1$ brings the phonon frequencies into agreement with experiment; for Ga we use $\alpha = \frac{5}{6}$. Note that the influence on the pair interactions is quite small.

Figure 1 shows the pair interactions for the trivalent metals. For Al the local empty-core potential with the core radius R_c fitted to the zero-pressure condition (R_c = 0.59 Å) and the optimized pseudopotential with $\alpha = 1$ lead to reasonably consistent results. The optimized pseudopotential with $\alpha = \frac{2}{3}$ yields a somewhat larger amplitude for the Friedel oscillations around the nearest-neighbor distance. In the pair-correlation function (Fig. 2) and in the static structure factor (Fig. 3) this is reflected in larger amplitudes in both $S(q)$ and $g(R)$, whereas both the empty-core potential and the optimized pseudopotential with $\alpha = 1$ yield an excellent agreement with experiment.

Ga illustrates the difficulties arising from an oversimplified form of the potential. We can adjust R_c such that the repulsive part of $\Phi(R)$ reflects the proper size of the atom — in this case the amplitude of the Friedel oscillations is too large and this results in a strongly distorted $g(R)$ and $S(q)$. If R_c is reduced such that the on-Fermi-sphere matrix element becomes smaller and hence the oscillations weaker, this leads to an underestimate of the effective size of the atom. A value of R_c = 0.44 Å is the best possible, but not entirely satisfactory, compromise for the structure of liquid Ga (see Figs. 1–3).

These difficulties are even more pronounced for the

heavy metals, as we have already shown in I for Sn and Pb. The optimized pseudopotentials lead to reliable pair potentials and accurate results for the liquid structure, but only if at least the ionic core is treated in a scalar relativistic approximation (Figs. 1–3). Again this is completely analogous to our results for Cd, Hg, Sn, and Pb. With the semirelativistic pseudopotentials we achieve a rather accurate description of the liquid structure. Note, however, that small kinks in $S(q)$ subsist at $q \sim 2k_F$ (at the foot of the first peak). This indicates that there is still a weak modulation of the structure by the Friedel oscillations, although it is difficult to see in the pair-correlation function.

The trend in the liquid structures appears also very clearly in the distribution of the bond angles, although the asymmetry of the first peak of the pair correlation function makes the definition of a nearest-neighbor bond somewhat ambiguous. If we define a nearest neighbor as having a distance shorter than the distance $R_{\min}$ of the first minimum of the pair-correlation function, we calculate coordination numbers of N_c=12.4, 14.8, 13.6, and 14.0 for Al, Ga, In, and Tl. If we determine the coordination number by integrating over the symmetric part of the first peak, we find N_c=10.1, 7.2, 8.6, and 9.1 for Al, Ga, In, and Tl. The difference of these numbers is a direct measure for the distortion of the atomic arrangement relative to a hard-sphere-like structure (where it is nonzero, but small). The distribution formed by all bonds up to $R_{\min}$ is shown in Fig. 4. Al, In, and Tl show a bond-angle distribution with peaks close to the icosahedral angles

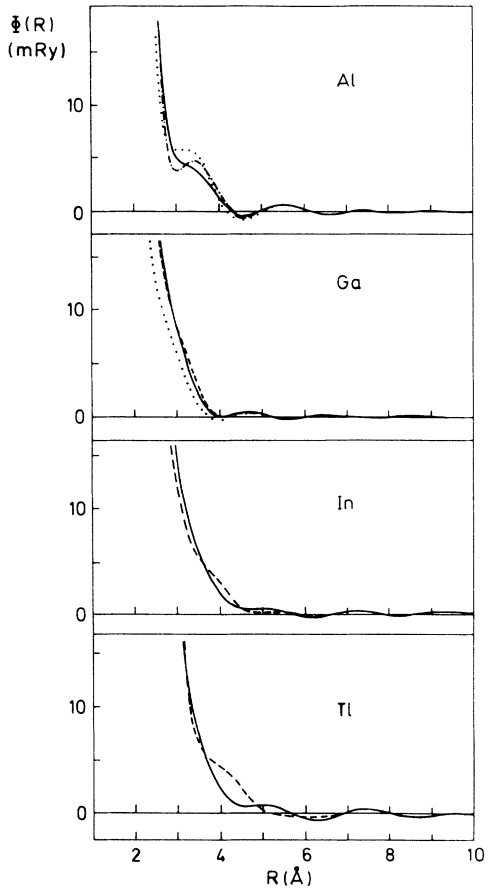

FIG. 1. Effective interatomic potentials for the trivalent metals. Dotted line, calculated with the local empty-core model potential; solid and dashed lines, optimized nonlocal pseudopotential calculated with relativistic and nonrelativistic core orbitals. The dot-dashed line for Al represents a potential calculated with a smaller valence-core exchange interaction (see text).

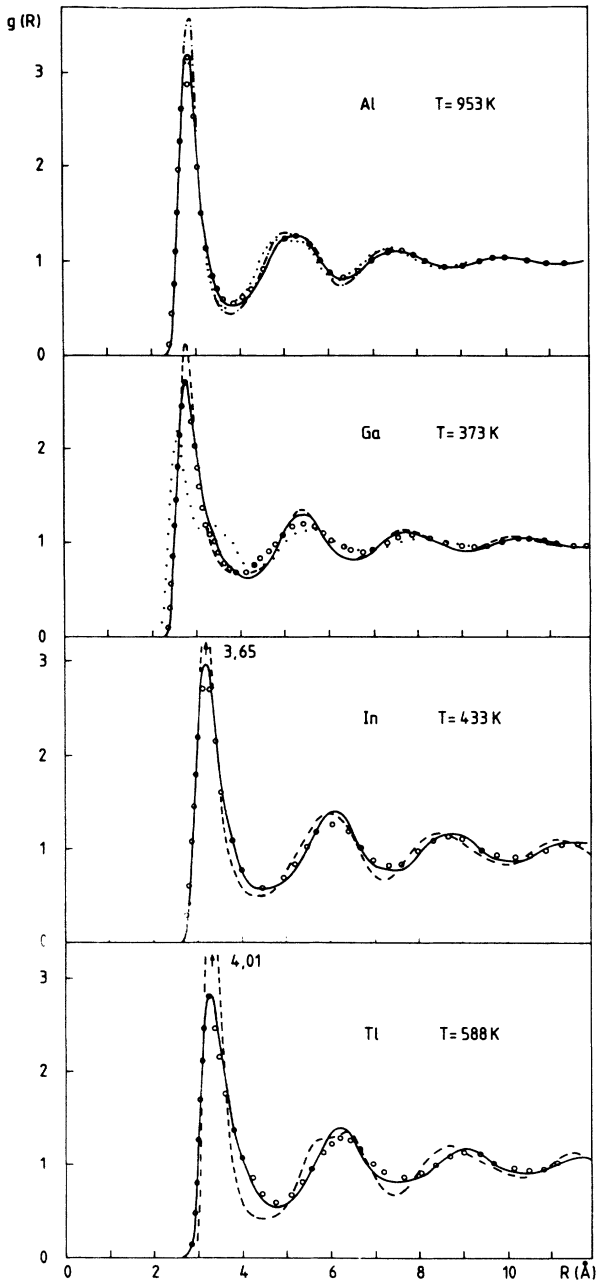

FIG. 2. Pair-correlation function $g(R)$ for the liquid trivalent metals, calculated with the potentials shown in Fig. 1 (same symbols). The open circles show the experimental results (Ga after Ref. 11, Al, In, and Tl after Ref. 3).

θ=63.5° and 114.5°, indicating an atomic arrangement that is essentially a polytetrahedral packing (the icosahedron being the ideal nearest-neighbor arrangement in a polytetrahedral structure). In liquid Ga the peaks are shifted to smaller bond angles and broadened. The distribution derived from the simulations with the local model potential are particularly diffuse and are similar to those calculated for *l*-Si and *l*-Ge (see I). This indicates that, like *l*-Si and *l*-Ge, *l*-Ga is considerably more disordered than normal liquid metals. However, there is also an important difference: in liquid Si the shortest bonds (with a maximal bond length equal to the covalent bond length) form angles distributed around the tetrahedral bond angle of θ=109°. These bonds represent a fraction of 25–30% of all nearest-neighbor bonds. In Ga we find no qualitative changes in the bond-angle distribution if we gradually restrict the maximum bond length. This indicates that the importance of covalent bonding effects is less important in *l*-Ga than in *l*-Ge (see our remarks on covalency and pair forces in I).

Note that the form of the potential calculated for Ga is in reasonable agreement with an empirical potential deduced from accurate neutron-diffraction data via an iterative inversion procedure.[25] The straightforward calculation of $\Phi(R)$ and the structure factor inversion result in a potential that is entirely repulsive around the nearest-neighbor distance and ascribe the anomalous structure of liquid Ga to the change of the curvature of $\Phi(R)$ around D_{cp}. In In and Tl the curvature must be completely monotonic in order to recover the more symmetric form of the structure functions. Of course such details depend rather sensitively on the various ingredients of the potential. It is therefore very gratifying that the calculations based on the optimized pseudopotentials extend and confirm the analysis based on the simple model potentials. In II, the same conclusion had been reached for the divalent metals. We have also repeated the construction of the potential and the molecular-dynamics simulations for liquid Si and Ge and find that the approach used for Al and Ga also yields very accurate liquid structures for these elements. Hence we obtain coherent results for all elements from groups II to IV.

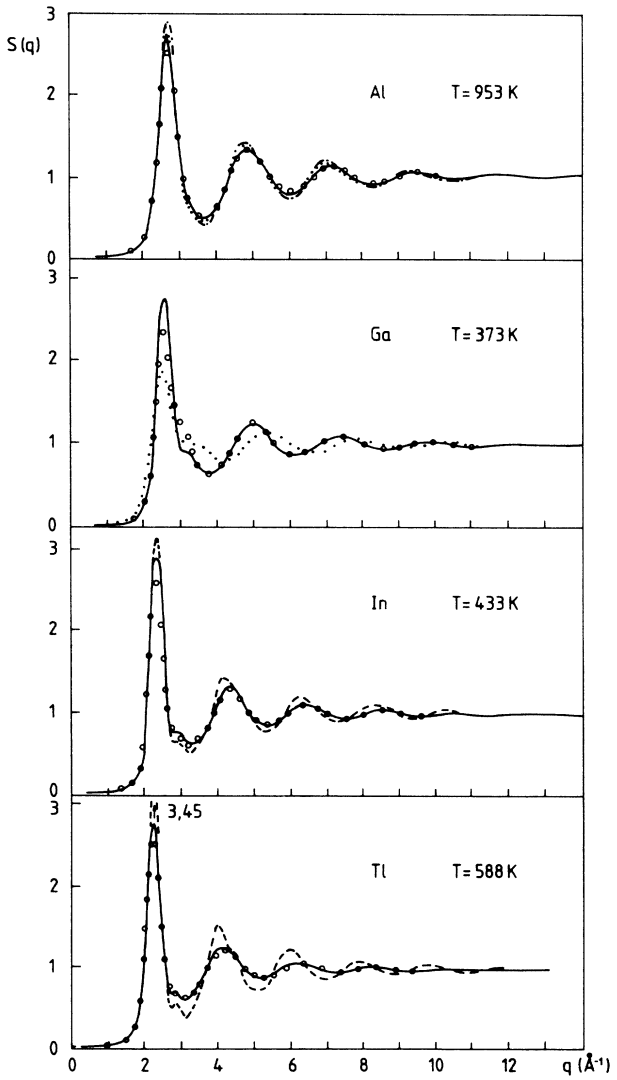

FIG. 3. Static structure factor $S(q)$ for the liquid trivalent metals. Same symbols as in Figs. 1 and 2.

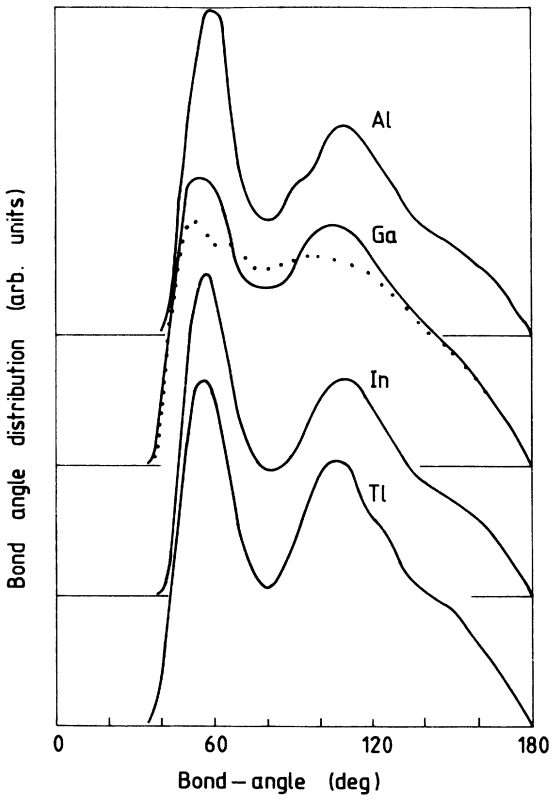

FIG. 4. Bond-angle distribution functions for the liquid trivalent metals. Same symbols as in Figs. 1 and 2.

III. ELECTRONIC STRUCTURE

In the following we discuss the electronic densities of states calculated using the linear-muffin-tin-orbital (LMTO) method[26,27] for supercells containing representative configurations of the liquid metals (see I and II for any technical details) and for the stable crystalline structures.

A. Aluminum

For both face-centered-cubic and liquid Al the calculations predict a DOS close to the free-electron parabola, the bandwidth being slightly reduced compared to the free-electron prediction (Fig. 5). The predicted narrowing of the band is in good agreement with the estimate derived from the photoemission spectra[4,28] (for a detailed comparison of the calculated photoemission intensities with experiment, see Sec. IV). The small structure in the crystalline DOS arises in a well-known way from the opening of gaps at the surfaces of the first, second, and third Brillouin zone. Some of this structure is also found in liquid Al; the first peak in the static structure factor acts as a smeared-out reciprocal-lattice vector. Although the s states are concentrated at the bottom of the band and the p states close to the Fermi edge, there is a large overlap characteristic for a free-electron band.

B. Gallium

Unlike in Al, big changes in the electronic DOS occur at the melting of Ga (Fig. 6). Body-centered-orthorhombic α-Ga (Ref. 29) has a strongly structured DOS with a deep minimum at the Fermi energy. The DOS minimum is well confirmed by photoemission studies;[30] the structure in the DOS is in good agreement with the optical spectrum of α-Ga.[31] These characteristic features are completely destroyed upon melting. Liquid Ga shows a nearly completely free-electron-like parabolic band with only a small kink 3 eV below E_F. This kink is also found in the measured ultraviolet-photoemission-spectroscopy (UPS) spectra. It indicates a more pronounced separation of the s and p states; it is a precursor of the pseudogap found in Ge and in the heavy elements from groups II to IV.

Clearly the changes in the electronic DOS reflect the drastic changes in the *short-range* order on melting (note that the total loss of *long-range* order has little effect on the electronic DOS of nearly all liquid metals). The partial covalent bonding character of the α phase (most evident in the deep DOS minimum at E_F) is destroyed on melting and this results in more metallic properties for the liquid.

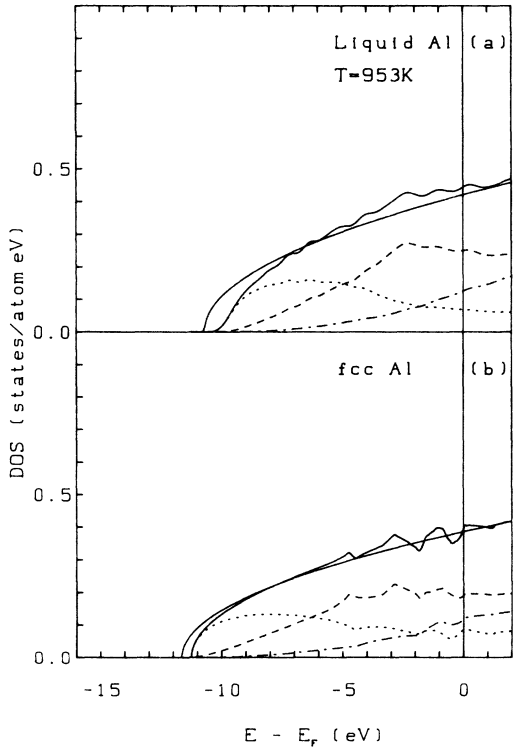

FIG. 5. Total and angular-momentum-decomposed electronic densities of states for liquid and face-centered-cubic Al. Solid line, total DOS; dotted line, s states; dashed line, p states; dot-dashed line, d states. The parabola shows the free-electron DOS.

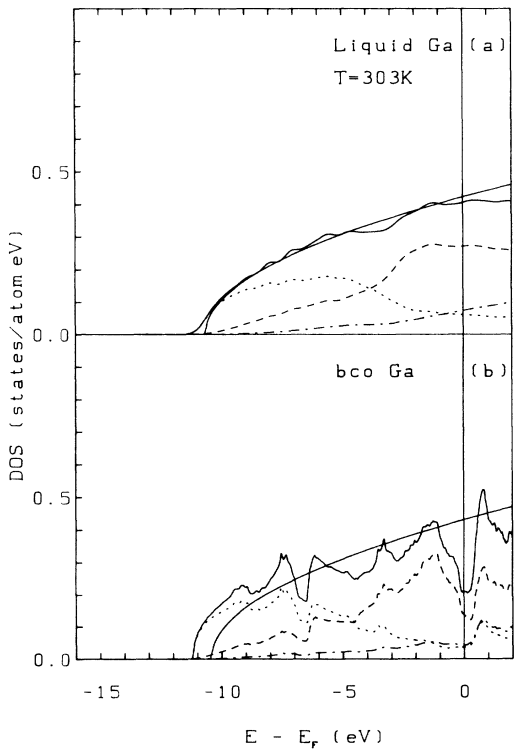

FIG. 6. Total and angular-momentum-decomposed electronic densities of states for liquid Ga and body-centered-orthorhombic α-Ga. Symbols as in Fig. 5.

C. Indium

Relativistic effects result in a lowering of the s-electron energy levels relative to the d states, so that in In the d states lie only 4 eV below the bottom of the conduction band. This complicates the electronic structure calculations. For crystalline In (face-centered-tetragonal) we have compared two sets of calculations, one with a frozen-core approximation for the $4d$ states, and one with a relaxed $4d$ band. We found the differences in the electronic DOS to be rather small (on the scale set by the energy resolution of our supercell calculation — see the discussion of the more technical aspects in I and II), so that the supercell calculations for the liquid have been performed in a frozen-core approximation for the $4d$ electrons.

The DOS of crystalline In is essentially parabolic, except that the relativistic lowering of the s states broadens the band over the free-electron value and the tetragonal distortion of the bands leads to a somewhat stronger structure in the DOS than in a cubic structure (Fig. 7). The DOS minimum at E_F tends to stabilize the tetragonal structure and we refer to the discussion in Refs. 12 and 13 as to how this relates to the form of the pair interaction. In indium there are only small changes in the short-range order on melting. As a consequence the electronic DOS's of the crystalline and of the liquid phase are very similar: we observe the same tendency to a broadening over the free-electron band and the same pronounced dip 2 eV below E_F separating the s- and p-dominated parts of the conduction band.

D. Thallium

As in fcc Pb, the valence band of hexagonal-close-packed Tl (Fig. 8) is split by a gap of 0.8 eV into a completely filled s band containing two electrons per atom and a p band close to the Fermi level. The lower edge of the s band is shifted below the bottom of the free-electron band.

The characteristic properties of the electronic DOS are preserved on melting: a pronounced pseudogap 3 eV below E_F separates a band containing exactly two electrons per atom and with predominant s character from a p band close to the Fermi level. The almost constant DOS around E_F in the liquid reflects the DOS minimum in the crystal, and the asymmetric form of the s electron DOS in the melt the form of the s band in a close-packed crystalline structure.

IV. PHOTOEMISSION INTENSITIES

The photoemission studies[4] of the liquid trivalent metals have shown that the energy distribution of the emitted photoelectrons depends strongly on the energy of the exciting photons. To profit from this information one has to calculate the variation of the photoioniza-

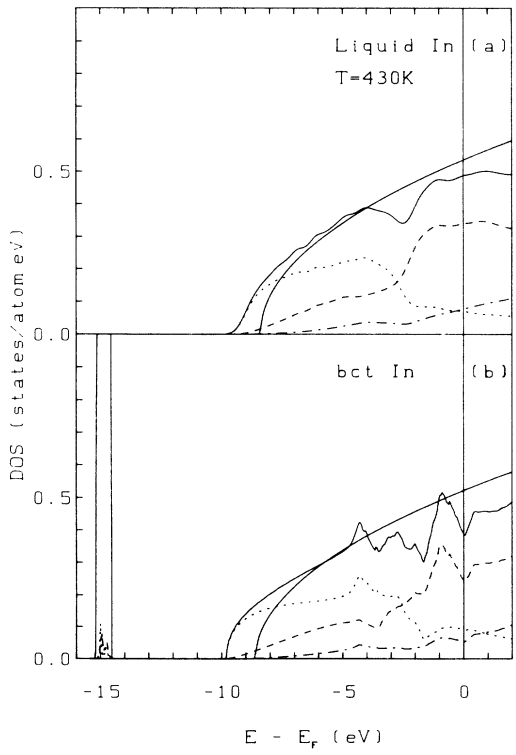

FIG. 7. Total and angular-momentum-decomposed electronic densities of states for liquid and face-centered-tetragonal In. Symbols as in Fig. 5.

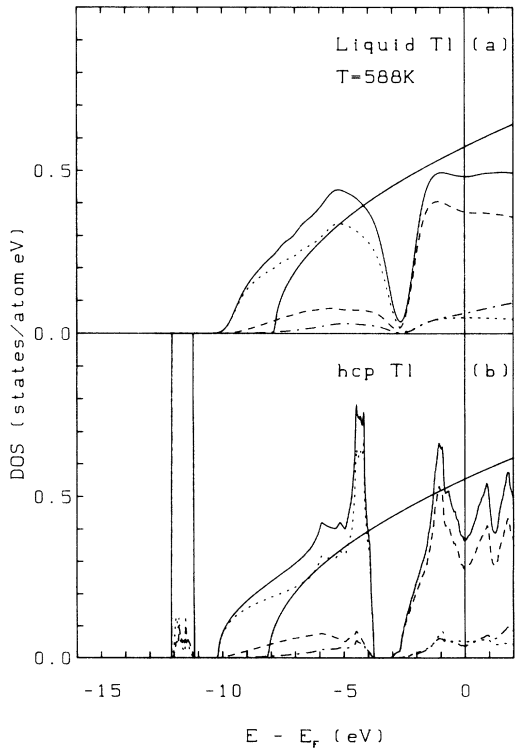

FIG. 8. Total and angular-momentum-decomposed electronic densities of states for liquid and hexagonal-close-packed Tl. Symbols as in Fig. 5.

tion cross section $\sigma_l(E,\hbar\omega)$ with the binding energy E and the angular moment l of the excited electron and with the energy $\hbar\omega$ of the photon. These partial photoionization cross sections can be calculated from the self-consistent one-electron potential in a single-scatterer final-state approximation.[32-35] For details, see II and Ref. 35.

A. Aluminum

Figure 9 shows the partial photoionization cross sections $\sigma_l(E,\hbar\omega)$ and the photoemission intensities $I(E,\hbar\omega) = \sum_l \sigma_l(E,\hbar\omega)n_l(E)$ for liquid Al , calculated for several photon energies in the x-ray photoemission spectroscopy (XPS) and the ultraviolet (UPS) energy range. For XPS energies the spectrum is dominated by the s states, with a small contribution of p states at low binding energies. The theoretical result is in quasiperfect agreement with experiment. The agreement extends even to details such as the small dip at 2.5 eV, which has also been found in the photoelectron spectrum of crystalline Al.[36] These structures have a double origin: the weak-structure-induced modulation of the free-electron DOS (see the discussion in Sec. III A) and the large difference in the $\sigma_l(E,\hbar\omega)$, $\sigma_s \gg \sigma_p$.

The UPS spectra are all of a triangular form, similar to the UPS spectra of Na (Ref. 35) and Mg.[2] The triangular shape arises from the increase of all partial photoionization cross sections with decreasing binding energy, which modifies the form of the spectrum (especially of its s-electron component) relative to the DOS. A variation of the photon energies affects mainly the relative weighting of the s, p, and d contributions without changing the form of the spectrum.

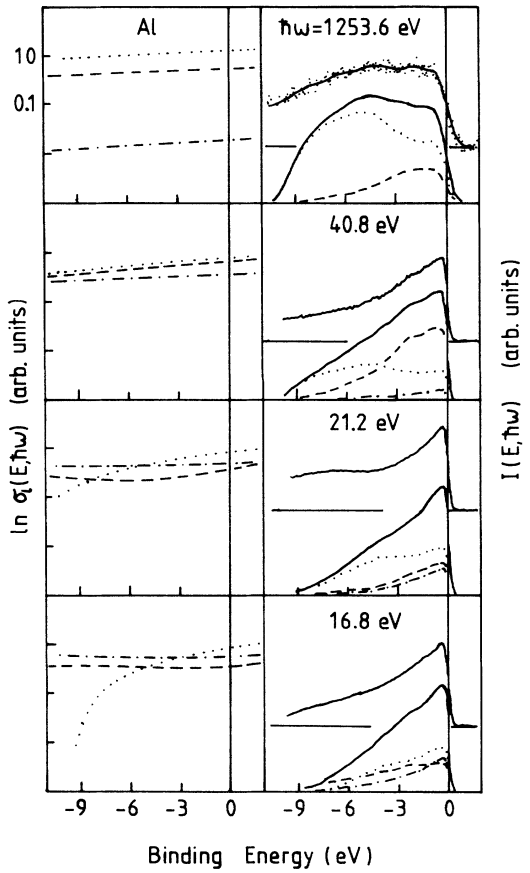

FIG. 9. Partial photoionization cross sections $\sigma_l(E,\hbar\omega)$ (dotted line, σ_s; dashed line, σ_p; dot-dashed line, σ_d) and photoemission intensity $I(E,\hbar\omega)$ (solid line, total; dotted line, s electron; dashed line, p electron; dot-dashed line, d electron contribution) for liquid Al at various energies of the exciting photon. For UPS energies the calculated intensity has been multiplied with a Fermi function, for the XPS spectrum the calculated intensity has been additionally Gaussian broadened (σ=0.50 eV) to account for the lower experimental resolution. The experimental results of Indlekofer *et al.* (Refs. 4 and 28) are shown for comparison. For the sake of clarity the zero of the experimental intensity has been shifted.

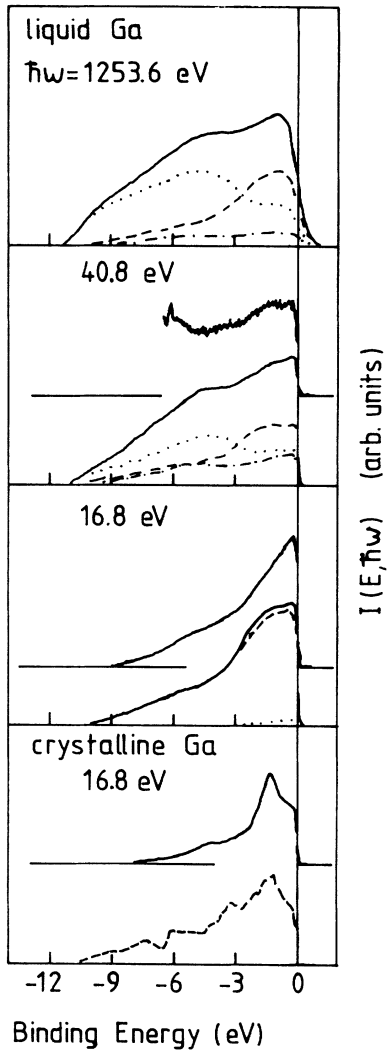

FIG. 10. Photoemission intensity $I(E,\hbar\omega)$ for liquid and crystalline Ga, cf. Fig. 9. For crystalline Ga the calculated partial p-DOS (cf. Fig. 6) is shown for comparison with the measured UPS spectrum. See text.

For liquid Al the $3p$ electron DOS can also be tested against the Al $K\beta$ soft-x-ray-emission spectrum.[37] Again the theoretical prediction is in full agreement with experiment.

B. Gallium

For Ga only UPS spectra have been measured. The strong changes in the electronic DOS at the Fermi level on melting are clearly reflected in the UPS spectrum (Fig. 10). When we compare the photoemission spectra for crystalline and liquid Ga, we must remember that the approach used for the calculation of the photoionization cross sections[32–35] involves the complete neglect of wave-number conservation. For the liquid this is acceptable at all photon energies as the wave number is not a conserved quantity. For the crystal this is acceptable if the energy of the exciting photon is much larger than the binding energy of the electron ($\hbar\omega \gg E$), i.e., only for XPS spectra. For the $\hbar\omega$=16.8-eV UPS spectrum of liquid Ga, we find that the spectrum is entirely dominated by the p states ($\sigma_p \gg \sigma_s, \sigma_d$) with a σ_p that depends only weakly on the binding energy. Tentativley we assume that the same holds for α-Ga [unfortunately no atomic photoionization cross sections are available for $4p$ and $4d$ electrons in Ga (Ref. 38)]. The important point is that both theory and experiment agree very nicely in the changes of the DOS near E_F on melting.

For liquid Ga, the spectra recorded with low photon energies again have a triangular shape. The strong changes in the electronic DOS at the Fermi level on melting are clearly reflected in the UPS spectrum (Fig. 10). At higher photon energies the exitation of s electrons becomes more important. This explains the flatter form of the spectrum, which approaches a free-electron shape, except for a slight dip at 3-eV binding energy, which indicates the incipient dehybridization of s and p states. Again we note good agreement between theory and experiment.

The spectra recorded with low photon energies again have a triangular shape. The strong changes in the electronic DOS at the Fermi level on melting are clearly reflected in the UPS spectrum (Fig. 10). At higher photon energies the exitation of s electrons becomes more important. This explains the flatter form of the spectrum, which approaches a free-electron shape, except for a slight dip at 3-eV binding energy, which indicates the incipient dehybridization of s and p states. Again we note good agreement between theory and experiment.

C. Indium and thallium

The UPS spectra of liquid In and Tl are characterized by a pseudogap 2 eV below the Fermi energy. The DOS minimum is particularly pronounced in the case of Tl where the pseudogap is seen to separate an s band from a p band (Figs. 11 and 12). The shape of the p band close to the Fermi edge is almost triangular at low photon energies. This contrasts with the spectrum of crystalline Tl whose form close to E_F reflects very clearly the DOS minimum (see Fig. 8). At higher photon energies the spectrum assumes a more rounded form — this is a good example that only a calculation of the variation of the cross sections with the photon and electron energies allows a reliable interpretation of the spectra.

The comparison with experiment is complicated by the onset of an Auger transition, which masks the lower edge of the band. With this restriction we observe again a very good agreement between theory and experiment.

V. CONCLUSIONS

This work completes the first *ab initio* investigation of the trends in the structural and electronic properties of the liquid polyvalent metals.

The increasing distortion of the structure factors and pair-correlation functions in the liquid divalent metals from Mg to Hg; the occurrence of a rather unique, loosely packed structure in liquid Ga, but then the return to

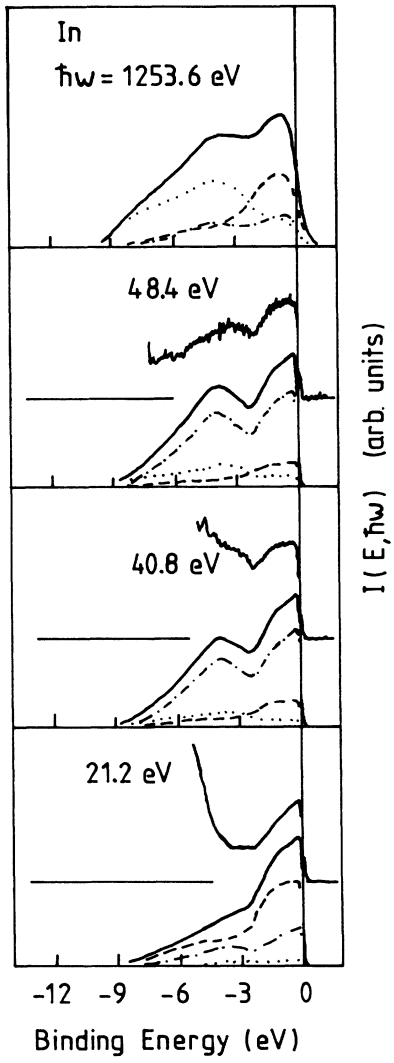

FIG. 11. Photoemission intensity $I(E,\hbar\omega)$ for liquid In, cf. Fig. 9.

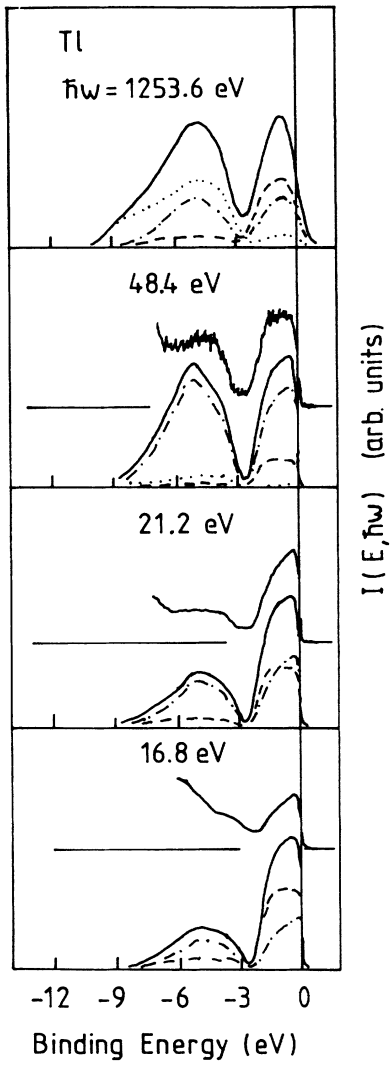

FIG. 12. Photoemission intensity $I(E,\hbar\omega)$ for liquid Tl, cf. Fig. 9.

more close-packed structures in In and Tl; the complex open structures of liquid Si and Ge and the transition to close-packed structures in Sn and Pb are found to arise from the modulation of the basic dense-random packing structures by the Friedel oscillations in the effective interatomic interactions and the damping of these oscillations in the heavy elements.

Of course these effects are closely related to the trends in the electronic structure. It is important to notice that the electronic structure of the elements that show the most pronounced deviation from a dense-random packing of spheres (Si,Ga) is essentially free-electron-like. This shows that our picture based on Friedel oscillations and hence metallic screening is basically correct. The amplitude of the oscillations is set by the on-Fermi-sphere matrix element of the electron-ion potential. We have shown that relativistic effects are important in understanding the reduction of the on-Fermi-sphere matrix element and the change to a soft-repulsive pair interaction in the heavy elements. A reduction of the matrix element for momentum transfers around $q = 2k_F$ is paralleled by an increase of the matrix element at smaller momentum transfers in the range $q \simeq (1 - 1.5)k_F$ (see Fig. 22 in I) close to the position of the first maximum in the static structure factor. We find that a sharp first peak in the static structure factor acts as a smeared-out reciprocal-lattice vector. If the electron-ion matrix element is large, this may lead to structure-induced minima in the electronic DOS. Such pseudogaps are found in the first-row elements Li and Be (see II and Ref. 35) where they are related to the strong nonlocality of the ionic pseudopotentials and in the heavy polyvalent metals Hg, Tl, and Pb (to a lesser degree also in Cd, In, Sn, and Ge), where the structure-induced pseudogap is enhanced by the relativistic s-p splitting.

We find that as a rule the electronic structure is rather similar to that of the crystalline phase. Notable exceptions are Ga, Si, Ge, and Sn, where the change in the electronic DOS reflects the change in the local atomic order on melting.

Our study also includes the alkaline-earth metals where we show that the electronic structure is strongly influenced by s-d hybridization. Liquid Ba must in fact be treated as a liquid transition metal.

It is a particular advantage of our technique compared to methods such as density-functional molecular dynamics[39] that it applies to d-bonded as well as s,p-bonded systems (besides it is also less expensive in computer time by about a factor of 10^2). First results for the molten transition metals are planned to be reported soon.[40]

ACKNOWLEDGMENTS

We thank Professor P. Weinberger and Dr. J. Redinger for the computer program used to calculate the photoionization cross sections. This work has been supported by the Fonds zur Förderung der wissenschaftlichen Forschung in Österreich (Austrian Science Foundation) under Project No. 7192. The numerical calculations were performed on an IBM 3090–400 VF of the Computer Center of the University of Vienna, supported by the IBM European Academic Supercomputer Initiative (EASI).

[1] W. Jank and J. Hafner, Phys. Rev. B **41**, 1497 (1990).
[2] W. Jank and J. Hafner, Phys. Rev. B **42**, 6926 (1990).
[3] Y. Waseda, *The Structure of Non-Crystalline Materials—Liquids and Amorphous Solids* (McGraw-Hill, New York, 1980).
[4] G. Indlekofer, P. Oelhafen, R. Lapka, and H. J. Güntherodt, Z. Phys. Chem. **157**, 465 (1988).
[5] G. Indlekofer and P. Oelhafen, Proceedings of the 7th In-

ternational Conference on Liquid and Amorphous Metals, edited by H. Endo [J. Non-Cryst. Solids **117&118**, 340 (1990)].
[6] J. D. Stroud and M. J. Stott, J. Phys. F **5**, 1667 (1975).
[7] A. H. Narten, J. Chem. Phys. **56**, 1185 (1972).
[8] A. Bizid, R. Cortes, A. Defrain, C. Regnaut, R. Bellisent, and G. Tourand, J. Chem. Phys. **77**, 779 (1980).
[9] M. C. Bellisent-Funel, R. Bellisent, and G. Tourand, J. Phys. F **11**, 139 (1981).
[10] S. Takeda, S. Harada, S. Tamaki, and Y. Waseda, J. Phys. Soc. Jpn. **55**, 3437 (1986).
[11] M. C. Bellisent-Funel, P. Chieux, D. Levesque, and J. J. Weis, Phys. Rev. A **39**, 6310 (1989).
[12] J. Hafner and V. Heine, J. Phys. F **13**, 2479 (1983).
[13] J. Hafner, *From Hamiltonians to Phase Diagrams*, Vol. 70 of *Springer Series in Solid State Sciences*, edited by P. Fulde (Springer, Berlin, 1987).
[14] J. Hafner and G. Kahl, J. Phys. F **14**, 2259 (1984).
[15] P. Vashishta and K. S. Singwi, Phys. Rev. B **6**, 875 (1972).
[16] S. Ichimaru and K. Utsumi, Phys. Rev. B **24**, 7385 (1981).
[17] N. W. Ashcroft, Phys. Lett. **23**, 48 (1966).
[18] W. A. Harrison, *Pseudopotentials in the Theory of Metals* (Benjamin, New York, 1966).
[19] J. Hafner, in *Cohesion and Structure*, edited by D. G. Pettifor and F. R. de Boer (North-Holland, Amsterdam, 1989), Vol. 2.
[20] J. A. Moriarty, Phys. Rev. B **8**, 1338 (1973); **6**, 4445 (1972).
[21] J. A. Moriarty, Phys. Rev. B **34**, 6738 (1986).
[22] J. A. Moriarty, Phys. Lett. A **131**, 41 (1988).
[23] J. Hafner, Z. Phys. B **22**, 351 (1975).
[24] J. Hafner, Z. Phys. B **24**, 41 (1976).
[25] L. Reatto, D. Levesque, and J. J. Weis, Phys. Rev. A **33**, 3451 (1986).
[26] H. L. Skriver, *The LMTO Method*, Vol. 41 of *Springer Series in Solid State Sciences*, edited by P. Fulde (Springer, Berlin, 1984).
[27] O. K. Andersen, O. Jepsen, and D. Glötzel, in *Highlights of Condensed Matter Theory*, edited by F. Bassani, F. Fumi, and M. P. Tosi (North-Holland, Amsterdam, 1985).
[28] G. Indlekofer, Ph.D. thesis, University of Basel, 1987 (unpublished).
[29] A detailed description of the structure of α-Ga is given in R. W. G. Wyckoff, *Crystal Structures*, 2nd ed. (Wiley, New York, 1962), Vol. I, p.22.
[30] F. Greuter and P. Oelhafen, Z. Phys. B **34**, 123 (1979).
[31] O. Hunderi and R. Ryberg, J. Phys. F **4**, 2096 (1974).
[32] T. Jarlborg and P. O. Nilson, J. Phys. C **12**, 265 (1979).
[33] H. Winter, P. J. Durham, and G. M. Stocks, J. Phys. F **14**, 1047 (1984).
[34] J. Redinger, P. Marksteiner, and P. Weinberger, Z. Phys. B **63**, 321 (1986).
[35] W. Jank and J. Hafner, J. Phys. Condens. Matter **2**, 5065 (1990).
[36] Y. Baer and G. Busch, Phys. Rev. Lett. **30**, 280 (1973); P. Steiner, H. Höchst, and S. Hüfner, in *Photoemission in Solids II*, Vol. 27 of *Topics in Applied Physics*, edited by M. Cardona and L. Ley (Springer, Berlin, 1979), p. 369.
[37] C. F. Hague, Phys. Rev. B **25**, 3529 (1982).
[38] J. J. Yeh and I. Lindau, At. Data Nucl. Data Tables **32**, 1 (1985).
[39] R. Car and M. Parrinello, Phys. Rev. Lett. **55**, 2471 (1985).
[40] J. Hafner, Ch. Hausleitner, and W. Jank (unpublished).